First-principles study of the superconductivity of MoB_2 under low pressure and its evolution under high pressure

Chao Zhou,[1] Hongyu Yu,[1,*] Zihan Zhang,[1] Zekun Yu,[1] Jinming Zhu,[1] Kuo Bao,[1,†] and Tian Cui[2,1]
[1]*State Key Laboratory of Superhard Materials, College of Physics, Jilin University, Changchun 130012, China*
[2]*Institute of High Pressure Physics, School of Physical Science and Technology, Ningbo University, Ningbo 315211, China*

(Received 19 October 2023; revised 22 December 2023; accepted 17 January 2024; published 5 February 2024)

Ever since it was found that MoB_2 holds the second-highest superconductive transition temperature (T_c, 32 K) amongst all known diborides, the argument on the donation of its two phases, the high-pressure α-MoB_2 phase (hexagonal, *P6/mmm*) and the low-pressure β-MoB_2 (rhombohedral, *R*-3*m*) has never stopped, because the phase-transition pressure is approximately 50 GPa higher than the pressure that superconductivity takes place. We simulated the phase transition and the possible superconductive properties of the two phases, and found that the ordered stacking arrangement ensures the *p-d* hybridization near the Fermi level and induces significant electron-phonon coupling, which actually influences the superconductivity. Therefore, the α-MoB_2 is the only phase that could be a superconductor. With our simulation, instead of further increasing, the T_c of MoB_2 would decrease slowly after reaching the maximum with a $d\,T_c/dp$ of -0.014 K/GPa, primarily due to the expected decrease and saturation of the electron-phonon coupling constant (λ) mainly contributed by Mo, along with the higher-frequency moments provided by B atoms under higher pressure. Therefore, in a certain transition-metal boride, it is not only the relatively high-frequency moments induced by B atoms, but also the stacking structure of them drives the electrons around transition-metal core in good symmetry and strengthens electron-phonon coupling, which leads to good superconductivity. Therefore, to manipulate boron-layer stacking arrangements might be an important angle to design and develop cutting-edge superconducting borides.

DOI: 10.1103/PhysRevB.109.064502

I. INTRODUCTION

Superconductors with high transition temperature (T_c) have long been the focus in condensed-matter physics and materials science. One promising path in searching high-T_c superconductors is to explore the materials with light elements [1–4], as they can provide high Debye frequency, which is directly related to the T_c according to the BCS theory [5]. Among these materials, metal diborides garner significant attention as superconductor candidates. Notably, MgB_2 was the first superconducting boride discovered [1], sparking the search for other superconductors among isostructural MB_2 (M = Al, Sc, Zr, Ta, and Y) [6–9]. Unfortunately, superconductivity is rare amongst them. However, MoB_2 stands out as a unique case with the second-highest T_c among known borides under pressure [10]. Notably, MoB_2 becomes superconductive above 20 GPa, with an increasing T_c to 32 K until 110 GPa. Additionally, a phase transition occurs from the low-pressure β-MoB_2 (rhombohedral, *R*-3*m*) to the high-pressure α-MoB_2 (hexagonal, *P6/mmm*) at approximately 68 GPa. The role of the two phases in its superconductivity remains an open question.

Efforts by Liu *et al.* [11] and Quan *et al.* [12] shed light on the superconductivity of α-MoB_2 under high pressure, and emphasized the significance of Mo-*d* electrons' contribution to the electronic structures and electron-phonon coupling (EPC) strength. Additionally, the presence of boron plays a crucial role in the system by providing substantial frequency moments. Nevertheless, the exact superconducting pairing mechanism in α-MoB_2 remains a subject of debate. Liu *et al.*'s study supported *s*-wave pairing [11], while Talantsev suggested the possibility of *d*-wave superconductivity [13]. WB_2 shares similarities with MoB_2; previous study suggested that defect structures during the phase transition might play a role in the occurrence of superconductivity [14]. Therefore, it is important to understand the superconducting behavior of MoB_2 under low pressure and investigate its evolution under higher pressure. To compare the experimental results and simulations, it would be helpful to understand the superconducting properties of MoB_2 under pressure.

In this work, we will investigate the stability evolution of the two phases of MoB_2, comparing their bonding properties, electronic structure properties, and EPC properties. Through these studies, we hope to figure out the key factors that influence the superconductivity of MoB_2. In addition, this work will help to reveal the evolution of T_c as a function of pressure.

II. METHOD

In this work, the structural relaxation and the electronic structure simulation are performed within a density-functional theory framework and the projector augmented-wave method [15] as implemented in the Vienna *Ab initio* Simulation Package VASP [16]. The Perdew-Burke-Ernzerhof generalized-gradient approximation deals with the exchange-correlation

*Corresponding author: yuhongyu@jlu.edu.cn
†Corresponding author: baokuo@jlu.edu.cn

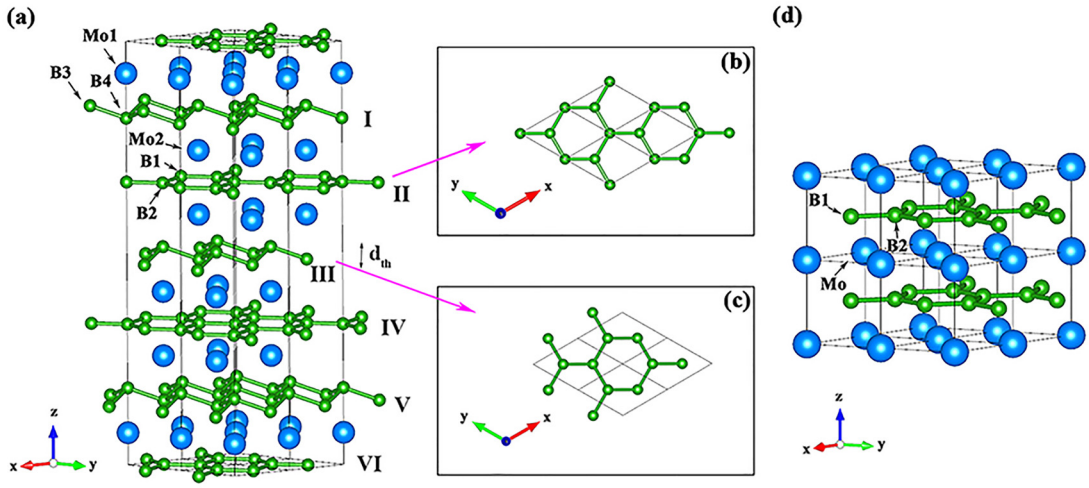

FIG. 1. (a) Crystal structure of β-MoB_2: the four kinds of different B atoms are labeled as B1, B2, B3, and B4, and the Mo atoms in different layers are labeled as Mo1 and Mo2. According to the differences in boron-layer thickness and stacking mode, there are six independent boron layers in the β-MoB_2, labeled with Roman numerals in sequential order from top to bottom. The plan view of (b) the planar boron honeycomb layer II, with (c) quasi-3D, buckled layer III, and d_{th} refers to the thickness of the buckled layer. (d) The crystal structure of α-MoB_2. The two neighboring boron atoms in the same layer are labeled as B1 and B2. The black lines depict the shape of the unit cell.

potential [17]. In the simulations, we set an energy cutoff as 600 eV for plane-wave basis and Gamma-centered **k**-mesh spacing as $2\pi \times 0.03$ Å^{-1}. Mo 4*s*, 5*s*, 4*p*, and 4*d* electrons are explicitly calculated, and the same as the B 2*s*, 2*p* electrons; that is, they are not included in the pseudopotential. The crystal orbital Hamilton population (COHP) [18] is calculated using the LOBSTER package. The density of states (DOS) simulation adopts the tetrahedron method with Blöch corrections. The subsequent lattice dynamics and EPC simulations were carried out by using the QUANTUM ESPRESSO (QE) package [19] with the optimized norm-conserving Vanderbilt pseudopotentials [20] and a plane-wave cutoff of 80 Ry. Here, we used an $18 \times 18 \times 18$ $\boldsymbol{k}$ -point grid and a $6 \times 6 \times 6$ $\boldsymbol{q}$ -point grid for the computation of the phonon spectrum of α-MoB_2, and for β-MoB_2, an $18 \times 18 \times 18$ $\boldsymbol{k}$ -point grid and a $3 \times 3 \times 3$ $\boldsymbol{q}$ -point grid were used. The postprocessing of the data obtained by VASP was also done with the help of VASPKIT [21].

III. RESULTS AND DISCUSSION

The structures of α-MoB_2 and β-MoB_2 are shown in Fig. 1. The main difference between the two phases is that the β-MoB_2 comprises a buckled boron layer, whereas the α-MoB_2 consists of a completely flat boron layer. And, we should address that even if the buckled boron layer would become flat in the β-MoB_2, the differences are still in the stacking arrangement of the structures. In the α-MoB_2 phase, the stacking arrangement between adjacent boron layers is mirror symmetric about the Mo layer, while in the β-MoB_2, the positions of boron atoms in the adjacent boron layer are staggered, as seen in Figs. 1(b) and 1(c). In the β-MoB_2, six independent boron layers differ in thickness and stacking arrangements. The flat and buckled boron layers are arranged alternately with each other, and every three layers have the same stacking arrangements. For example, the plan views of boron layers I and IV are identical, but their thicknesses differ. Similarly, in the case of Mo atoms, they are arranged in a staggered fashion that alternates every two layers and forms flat layers. Therefore, the transition from the β-MoB_2 to the α-MoB_2 is accompanied with decreased boron-layer thickness and slip between the different layers. This process is crucial for understanding the superconducting behavior of the low-pressure phase and will be further discussed afterward.

We optimized the bulk α-MoB_2 and β-MoB_2 under different pressures, and the calculated lattice parameters along with pressure are shown in Figs. 2(a) and 2(b). Compared with the experimental data from Ref. [10], the evolution of the lattice parameters of β-MoB_2 under pressure is consistent, and those of α-MoB_2 are acceptable under high pressure. However, the lattice parameter *c* of α-MoB_2 prepared at the ambient pressure is 3.07 Å [22,23]; it might be 3.3 Å according to our simulation, which could be explained with boron defects as in previous reports on AlB_2-type WB_2 and MoB_2 [24]. Furthermore, an insightful observation from Fig. 2(c) reveals that the enthalpy of α-MoB_2 becomes lower than that of β-MoB_2 beyond 70 GPa. This signifies a notable phase transition, indicating that the β-MoB_2 will undergo transformation into the α-MoB_2 at around 70 GPa. It is consistent with the former experiment, where a mixture of α-MoB_2 and β-MoB_2 started to appear after 68 GPa [10]. Our simulation also shows that α-MoB_2 would be dynamically stable after 20 GPa, which could be regarded as the lowest edge of its stability. (see Fig. S1 in Supplemental Material [25]). The thickness of the buckled boron layer in β-MoB_2 shown in Fig. 1(c) remains around 0.6 Å and almost unchanged with increasing pressure, as shown in the inset of Fig. 2(d). Within the phase transition, if only the buckled layers collapse, which leads to a volume collapse around 2 Å^3 per formula unit at 70 GPa. Actually, the transition from the β-MoB_2 to the α-MoB_2 only leads to a volume reduction of approximately 1 Å^3 per formula unit. Under pressure, there is a competition between the reduction of the boron layer thickness and the slip of the

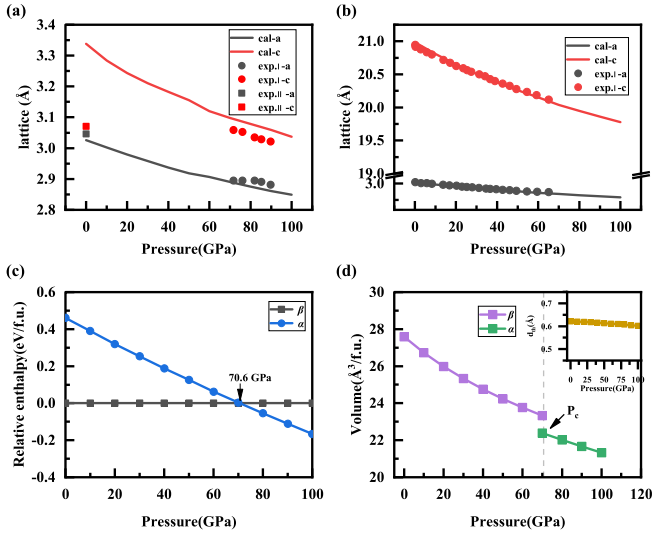

FIG. 2. (a), (b) The simulated lattice parameters of α- and β-MoB_2, respectively, within $0 \sim 100$ GPa, compared with the experimental values. "exp. I" refers to the experimental data from Ref. [10], which provide lattice parameters of the two phases before and after the phase transition under high pressure, and "exp. II" refers to the experiment in Ref. [28], which directly provides the lattice parameters of α-MoB_2 synthesized. (c) The relative enthalpy of α-and β-MoB_2 under different pressure; (d) the evolution of the volume of both phases; the P_c denotes the pressure at which the phase transition takes place, where an evident volume collapse could be observed before and after the structural phase transition. The inset in (d) is the thickness of the buckled boron layer in the β- MoB_2 with the pressure, and it can be seen that it only alters slightly in this large pressure variation.

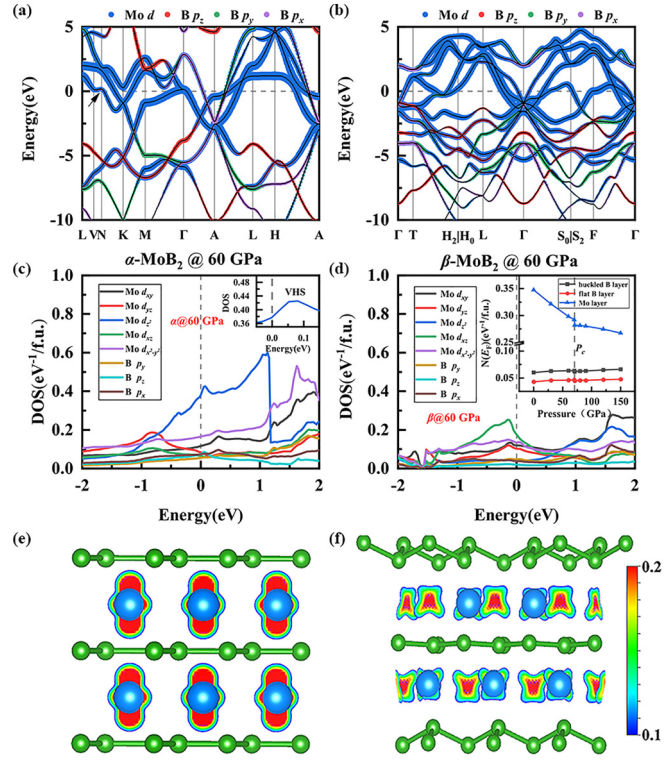

FIG. 3. (a) Projected band structures of α-MoB_2, and (b) β-MoB_2 at 60 GPa. The colorful dots represent the contributions of the corresponding orbitals, as shown in the legend. The size of the colorful dots represents the weight of their corresponding orbitals. The localized small flat band with the p-d hybridization was denoted by the arrows. (c) and (d) are the partial density of states (PDOS) of α-MoB_2, and β-MoB_2 at 60 GPa. A closeup of the PDOS of Mo-d_{z^2} orbitals around the VHS is given in the inset of (c). The inset of (d) shows the variation in the PDOS for different layers of β-MoB_2 under the influence of pressure. (e) and (f) are the charge densities in real space resulting from the band decomposition of α-MoB_2 and β-MoB_2 within the range of $[E_F - 0.5, E_F + 0.5]$ eV, and the unit of charge density is $e^{-1}/\text{Å}^3$.

boron layer, and the latter potentially leading to an expansion of the volume per formula unit, which might be the answer for the volume dilemma.

As observed as in Ref. [10], T_c within the β-MoB_2 significantly increases under low pressure, followed by transformation to the α-MoB_2. And, T_c continues to rise after the phase transition; the increment rate slows down. The superconducting mechanism of α-MoB_2 under high pressure has been extensively studied, but the low-pressure β-MoB_2 and its phase-transition process remain unclear and is one of our chief questions to be answered. First, we focused on the differences between them in terms of bonding properties. We compared the integrated projection of the crystal orbital Hamilton population (-IpCOHP) for the two phases at 70 GPa (shown in Table SI [25]). We found that there were almost no differences in their bonding characteristics, and the primary distinctions between the two phases present in the electronic structures. Therefore, we conducted an investigation on the low-pressure superconductivity mechanism before the phase transition, and we selected both phases at 60 GPa for their electronic structure simulation. The band structures of both phases at 60 GPa are provided in Figs. 3(a) and 3(b), and the corresponding PDOS of Mo-d orbitals and B-p orbitals are also provided in Figs. 3(c) and 3(d). According to the study by Liu et al [11]., there are Van Hove singularities (VHS) at the $\boldsymbol{k}$ -point V and N in the band structure of α-MoB_2, which is accompanied by p-d hybridization, leading to the softening of acoustic phonons in the phonon spectra. Previous studies also suggested that p-d hybridization can cause phonon softening in various materials with transition-metal atoms, and this was always linked to high-temperature superconductivity [26,27]. In α-MoB_2, the hybridization of Mo-d and B-p orbitals at the VHS could soften Mo-derived low-frequency phonon modes and cause a strong EPC strength, similar to the orbital hybridization of La f and H1 s in LaH_{10} [28]. As to the β-MoB_2, as illustrated in Fig. 3(d), the overall $N(E_F)$ is relatively low compared with the α-MoB_2's, and it is predominantly composed of Mo-d electrons. To further assess contributions from different layers within the β-MoB_2, $N(E_F)$ is projected onto the buckled boron layer, the flat boron layer, and the molybdenum layer, as shown in the inset of Fig. 3(d). Concerning the molybdenum layer dominant contribution, the $N(E_F)$ decreases with increasing pressure; on the contrary, the boron layer shows a gradual upward trend. It is noteworthy that at around 70 GPa, there is a sudden change in the $N(E_F)$, consistent with the observed phase transition from β-MoB_2 to α-MoB_2.

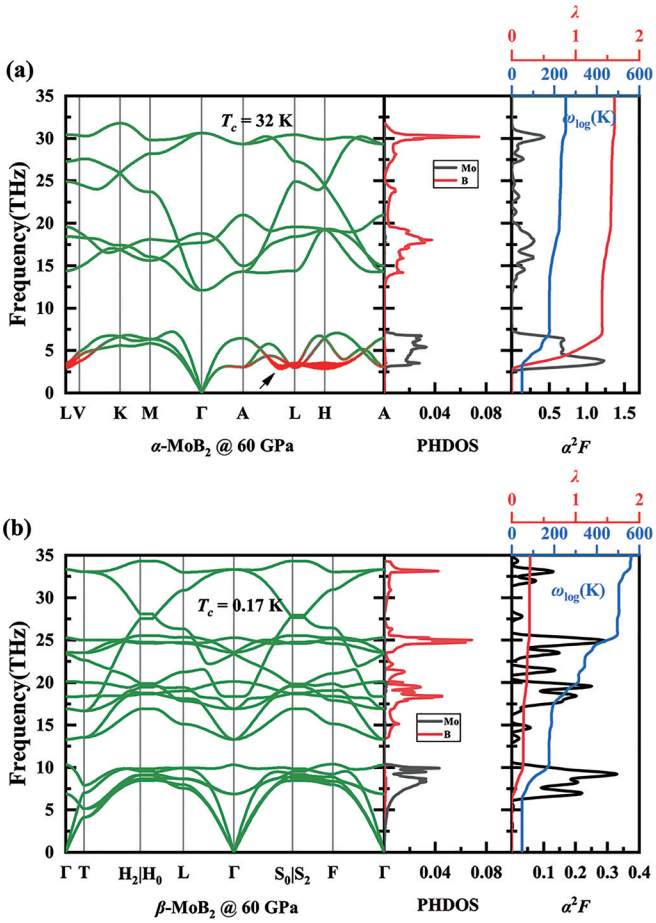

FIG. 4. The phonon band structure, phonon DOS (PHDOS), EPC constant $\lambda(\omega)$, logarithmic average phonon frequency $\omega_{\log}$, and Eliashberg spectral function $\alpha^2F(\omega)$ of (a) α-MoB_2 under 60 GPa, and (b) β-MoB_2 under 60 GPa. The size of the red circles on the dispersion curve is proportional to the EPC strength $\lambda_{q\eta}$. $\lambda_{q\eta}$ is the EPC strength for the mode η at wave vector $\boldsymbol{q}$.

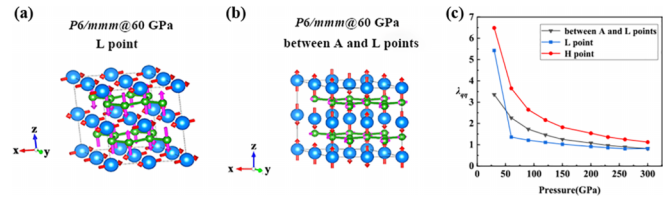

FIG. 5. The picture depicts the vibrational modes (a) at the L point and (b) between the A and L points in the $P6/mmm$ structure at 60 GPa. And the vibrational modes at the H point is similar as that at the L point, involving both phonon modes within the Mo layer plane and modes outside the boron layer plane. However, the vibrations of adjacent atoms of the same type are in opposite directions; and (c) illustrates the partial EPC constant $\lambda_{q\eta}$ for these three soft modes under pressure.

Then, to better analyze the differences near the E_F between the two phases, we extracted the charges from the band structure in the energy range of [$E_F - 0.5$, $E_F + 0.5$] eV into real space, as shown in Figs. 3(e) and 3(f). It can be seen that in both phases, the Mo-d orbitals contribute significantly to $N(E_F)$. However, in β-MoB_2, the $N(E_F)$, primarily contributed by its d_{xz} orbitals near the E_F, shows a smaller value than the α-MoB_2, where Mo-d_{z^2} orbitals predominantly occupy its $N(E_F)$. Furthermore, for the β-MoB_2, the shape of the charge distribution near the E_F is nonuniform and bears bad symmetry, which might not contribute to EPC strength much. Additionally, we calculated the net atomic charges with the density-derived electrostatic and chemical method [29]. At the same pressure, the Mo atoms in the α-MoB_2 lose more electrons than the β-MoB_2 (see Fig. S2 in Supplemental Material [25]). This also implies that flat boron layers in the α phase are more likely to accumulate charge with pressure increasing.

We calculated the phonon spectra using density-functional perturbation theory [30] to compare the superconducting properties of the two phases directly. Figures 4(a) and 4(b) show the phonon dispersions, phonon density of states (PHDOS), and the Eliashberg function $\alpha^2F(\omega)$ of both phases. There is a phonon gap in each phonon band structure between high-frequency optical branches and low-frequency acoustic branches in both phases. The acoustic and optical modes of both phases are mainly contributed by Mo and B atoms, respectively, as seen in PHDOS. There are some obvious phonon soft modes in α-MoB_2, as indicated by an arrow in Fig. 4(a) near the L and H points in the lowest acoustic branch. These modes manifest a considerable EPC strength, reflecting the strong electron-phonon interactions. Furthermore, we compared the vibrational modes of the corresponding phonon soft modes in the α-MoB_2 as shown in Fig. 5. In the α-MoB_2, two kinds of modes contribute significantly. One involves the in-plane phonon mode of Mo atoms and the out-of-plane phonon mode of B atoms, predominantly present near the L and H points. The other comprises the out-of-plane phonon mode of Mo atoms and the in-plane phonon mode of B atoms, occurring around the soft modes between the A and L points. Subsequently, we computed the evolution of the partial EPC constant $\lambda_{q\eta}$ for these three soft modes under pressure as shown in Fig. 5(c). It is obvious that at low pressure, the primary contributions come from the in-plane phonon mode of Mo atoms and the out-of-plane phonon mode of the B atoms. It is these phonon modes that lead to a strong EPC strength ($\lambda > 1.5$) under low pressure. The soft modes at the H point always exhibit a high contribution to λ, but as the pressure increases, the contributions from these soft modes become comparable.

It should be noted that the phonon soft modes in the α-MoB_2 are robust under pressure, because they are associated with low-pressure phonon instability (see Fig. S1 in Supplemental Material [25]). As the crystal becomes stable and the imaginary frequency disappears under pressure, the soft modes remain and contribute significantly to the EPC. Figure 4 also gives the Eliashberg function $\alpha^2F(\omega)$, the EPC constant $\lambda(\omega)$, and the logarithmic average frequency moment $\omega_{\log}$ as a function of phonon frequency. With the substantial value of λ at α-MoB_2 under low pressure, we utilize the Allen-Dynes modified McMillan equation to calculate T_c [31]:

$$T_c = \frac{f_1 f_2 \omega_{\log}}{1.2} \exp\left[-\frac{1.04(1+\lambda)}{\lambda - \mu^*(1+0.62\lambda)}\right], \quad (1)$$

where the f_1 and f_2 are strong-coupling correction parameters, and μ^* is typically determined by fitting the calculated observables to experimental data or by accepting typical values (e.g., ∼0.10–0.15) from previous fitting results [32]. In this study, we adopt a value of $\mu^* = 0.1$ for better comparison with the experiment. With obtained λ =1.6 for its strong coupling as mentioned above, $\omega_{\log} = 246.5$ K, and $\mu^* = 0.10$, ($f_1 = 1.02$, $f_2 = 1.06$); the T_c is estimated to be 32.2 K for α-MoB_2 at 60 GPa, while, β-MoB_2's T_c is 0.17 K, and there are no soft modes in its phonon spectra, which could be considered nonsuperconductivity. However, the T_c of MoB_2 is about 22.5 K at 60 GPa, and only β-MoB_2 was detected in this range at this pressure, which was indicated in the x-ray diffraction (XRD) [10]. Meanwhile, the observed superconductivity is solely attributed to the presence of metastable α-MoB_2 under low pressure according to our work. The coexistence of α-MoB_2 and β-MoB_2 might occur even under low pressure, despite the absence of α-MoB_2 detection. Given that α-MoB_2 demonstrates a noteworthy T_c under low pressure, the experimental T_c under lower pressures may be influenced by the contribution of α-MoB_2, even if its concentration is too small to be detected with XRD. And, we should note that nonstoichiometric-induced superconductivity is quite evident in transition-metal diborides (TMDBs) [33–39], and it was always thought that the defects in β-MoB_2 were the reason for its conductivity [14]; these are beyond this study. Similar challenge occurs in the experiments on WB_2 at comparative simulations, where the flat boron layers are considered the key to good superconductivity [40]. A good understanding on flat boron layer would be helpful in understanding superconductivity under low pressure.

As we mentioned before, the transition from the β-MoB_2 to the α-MoB_2 is characterized by the flattening of the boron layers and the slip between different layers. We can further analyze the changes in superconductivity by implementing adjustments to each phase: for example, by reducing the thickness of the boron layer in the β-MoB_2 or making one of the boron layers slightly buckled in the α-MoB_2. Then, we artificially manipulated both phases at 60 GPa by reducing the thickness of the buckled boron layers in the β-MoB_2 to 0.3 Å, without altering their stacking arrangements, and creating a buckled boron layer in the α-MoB_2, with a thickness of about 0.17 Å which can be seen in Figs. 6(a) and 6(b). Then, we calculated their phonon spectra, shown in Figs. 6(c) and 6(d), to study their dynamic stability. By reducing the boron-layer thickness in the β-MoB_2, we found that it is hardly superconductive, although it remains stable with the optical and acoustic branches closed. In contrast, in the α-MoB_2, by making one of the boron layers buckled to a thickness of 0.17 Å, its symmetry will degrade to P-3m1, and will still be stable with a T_c as high as 32.6 K. And, we have to note that we also attempted enlarge the thickness to 0.3 Å, and the structure became unstable. The DOS and band structures of the P-3m1 phase can be found in Fig. S3 in the Supplemental Material [25]. It is evident that the $N(E_F)$ is also primarily occupied by the Mo-d_{z^2} orbitals, and p-d hybridization is observed in the band structure. When examining the charge density near the E_F, similar to previous findings, although boron layers are buckled in the distorted α-MoB_2, the charge density maintains at good symmetry.

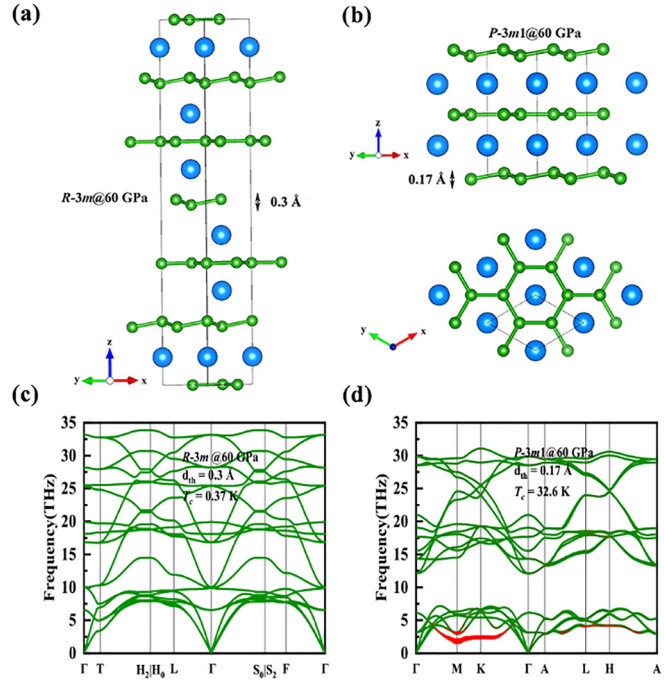

FIG. 6. (a) Shows the structure of the β-MoB_2 at 60 GPa, with an artificially changed thickness of the buckled boron layer to 0.3 Å. (b) Illustrates the structure with P-3m1 symmetry obtained by transforming one of the flat boron layers in the α-MoB_2 to a buckled one, with a thickness of 0.17 Å and a regular stacking arrangement when viewed from the top. The phonon spectra and the relevant EPC properties are presented in (c) and (d). The size of the red circles on the phonon spectra is proportional to the EPC strength $\lambda_{q\eta}$. For the structure with P-3m1 symmetry, the selected ***k***- and ***q***-point grids for calculating the phonon spectrum are 20 × 20 × 12 and 5 × 5 × 3, respectively.

Based on the above facts, we could draw the conclusion that the ordered stacking of boron layers introduces the superconductivity in MoB_2 as the stacking arrangement in α-MoB_2. This sandwichlike stacking arrangement forms a Mo-centered ligand field, and results in the high contribution from Mo-d_{z^2} orbitals at $N(E_F)$, which is favorable for hybridization with the p orbitals of B atoms, and leads to a significant λ. Even when the flat boron layers become buckled, the stacking way along the z axis remains unchanged. However, if a slip took place between the layers, the ligand field would be disrupted, and the superconductivity would be broken. This can also be observed in the Supplement Material, Fig. S4 [25]. In comparison to the previously mentioned P-3m1 phase, where the buckling of the boron layers maintains its T_c at 32.6 K, there is almost no change when compared to the original α-MoB_2 at 60 GPa. However, a slip of approximately 0.25 Å in half of the Mo layers in α-MoB_2@60 GPa results in a decrease of ∼5 K in its T_c. Therefore, the stacking arrangement of layers determines the superconductivity in MoB_2 and similar compounds, rather than the thickness of the boron layers. The contribution of d electrons on the $N(E_F)$ distinguishes MoB_2 from other AlB_2-type TMDBs, such as NbB_2, whose Nb-d_{z^2} orbitals do not contribute to its $N(E_F)$ much, and its T_c is relatively low (0.62 ∼ 9 K) [41–43]. On the contrary,

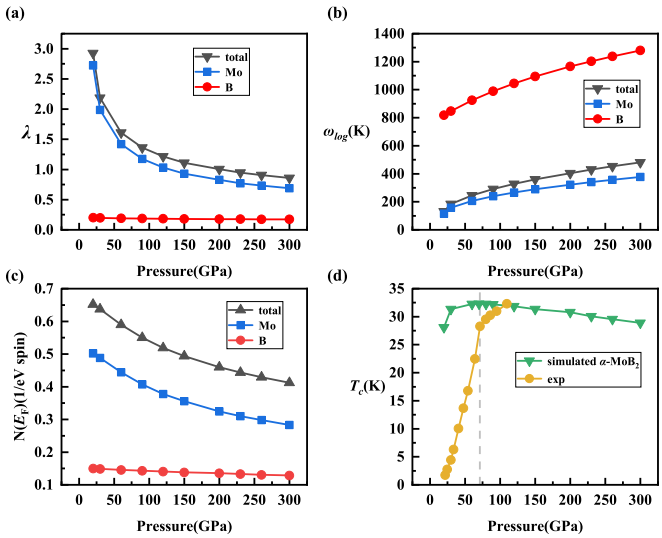

FIG. 7. The (a) λ, (b) $\omega_{\log}$, (c) $N^{\uparrow}(E_F)$, and (d) T_c of α-MoB_2 vary along with pressure, where the Coulomb potential μ^* is 0.10. The contributions from Mo and B are also shown in blue and red, respectively. In (d), the gray dashed line represents the experimental phase-transition boundary. The data of T_c from experiment could be found in Ref. [10].

the good superconductor, AlB_2-type WB_2, is isoelectronic to MoB_2 [40], whose W-d_{z^2} orbitals dominate the $N(E_F)$. The relevant results are presented in Fig. S5 [25] in the Supplemental Material. Therefore, enough d electrons and their high contributions to $N(E_F)$ are of great importance for the superconductivity.

We calculated the evolution of superconducting properties of the α-MoB_2 under higher pressures and calculated the EPC parameters of Mo and B atoms based on their respective primary contributions to the acoustic and optical branches as shown in Fig. 7, which would enable us take a comprehensive view on MoB_2's superconductivity. The EPC constant λ of α-MoB_2 at 20 GPa is 2.9, which is a relatively substantial value, mainly due to the significant EPC contribution near the soft modes of the acoustic branches. Then, as pressure increases, λ decreases and slows down under higher pressures. The main contribution of λ comes from Mo, while the contribution of λ from boron almost does not change with pressure. The $N(E_F)$ also shows a similar evolution trend, which indicates that the λ positively correlates with $N(E_F)$. So, the reduction in the $N(E_F)$ of d electrons under pressure is the primary cause for the decreased value of λ. As the pressure increases, the value of λ decreases, while the value of $\omega_{\log}$ increases. The optimal pressure for achieving the highest T_c is found to be around 70 GPa with our simulation, which corresponds to the experimental phase-transition point, and the T_c is approximately 32.2 K. And, T_c starts decreasing as the pressure rises further. Specifically, between 70 and 300 GPa, the value of d T_c/dP is ~ -0.014 K/GPa, much smaller than ~ -1.6 K/GPa of MgB_2 [44]. It suggests that pressure does not impact the T_c of the α-MoB_2 much after its maximum. It is because the boron layers continue to contribute to the frequency moments significantly, which enhances the overall frequency moments of the system as pressure increases, and λ approaches saturation. The T_c reaches a maximum of 32 K under 110 GPa experimentally [10]; while the value of maximum T_c is closely aligning with our simulation result, the corresponding pressures are, however, quite different. The distinction might be attributed to the assumption of perfect crystalline α-MoB_2, and phase mixing and the formation of some defect structures could lead to some incomplete superconductivity under low pressure. And the underestimation on the pressure effects on λ may also lead to the different pressure with the T_c maximum. Analytically, the value of λ shows great influence on T_c, and the underestimation on it could also lead to this dilemma of the pressure-T_c relation.

IV. CONCLUSIONS

We explored the stability of the two phases of MoB_2 and determined that the phase transition occurs at 70.6 GPa, and α-MoB_2 might be stable at the pressure as low as 20 GPa. With the comparison on the electronic structures and EPC properties between the two phases, we found that the correlation between the superconductivity of the low-pressure phase and that of β-MoB_2 is weak. In contrast, the high T_c of α-MoB_2 was observed under low pressure, and we also analyzed and compared the contributions of different soft phonon modes in α-MoB_2. Furthermore, we studied their EPC properties by artificially modifying the thickness of the buckled boron layer in the β-MoB_2 and inducing buckling in one of the boron layers in the α-MoB_2. We found that the stacking arrangement of the boron layers influenced the superconductivity predominantly, rather than their thickness. Therefore, the superconducting behavior under low pressure may arise from a subtle slip of the boron layers, which might hardly be measured with XRD. This slipping facilitates a sandwichlike stacking arrangement, creating a ligand field centered around Mo. Such a configuration could be a crucial factor inducing superconductivity in MoB_2. The study on the high-pressure T_c reveals that T_c does not continue to increase under higher pressures; instead, it would decrease slowly at a rate of -0.014 K/GPa after its maximum, which is attributed to the decreasing contribution of Mo to λ. Meanwhile, the boron layers are anticipated to offer significant frequency moments under higher pressure. In future research and design of boride superconductors, attention should be focused on the spatial structure of boron, especially the stacking relationships between different boron layers. Additionally, the selected metal atomic orbital spatial distribution should be relatively conducive to coupling with the ligand field formed by boron.

ACKNOWLEDGMENTS

This work was supported by the National Key R&D Program of China (Grants No. 2018YFA0703404 and No. 2017YFA0403704), National Natural Science Foundation of China (Grants No. 11774121 and No. 91745203), National Key Research and Development Program of China (Grant No. 2016YFB0201204), and Program for Changjiang Scholars and Innovative Research Team in University (Grant No. IRT_15R23). The calculations were performed at High Performance Computing Platform of Nanjing University of Aeronautics and Astronautics.

[1] J. Nagamatsu, N. Nakagawa, T. Muranaka, Y. Zenitani, and J. Akimitsu, Nature (London) **410**, 63 (2001).

[2] A. Drozdov, M. Eremets, I. Troyan, V. Ksenofontov, and S. I. Shylin, Nature (London) **525**, 73 (2015).

[3] A. P. Drozdov, P. P. Kong, V. S. Minkov, S. P. Besedin, M. A. Kuzovnikov, S. Mozaffari, L. Balicas, F. F. Balakirev, D. E. Graf, V. B. Prakapenka *et al.*, Nature (London) **569**, 528 (2019).

[4] E. Snider, N. Dasenbrock-Gammon, R. McBride, M. Debessai, H. Vindana, K. Vencatasamy, K. V. Lawler, A. Salamat, and R. P. Dias, Nature (London) **588**, E18 (2020).

[5] J. Bardeen, L. N. Cooper, and J. R. Schrieffer, Phys. Rev. **108**, 1175 (1957).

[6] H. Rosner, W. E. Pickett, S.-L. Drechsler, A. Handstein, G. Behr, G. Fuchs, K. Nenkov, K.-H. Müller, and H. Eschrig, Phys. Rev. B **64**, 144516 (2001).

[7] J. S. Slusky, N. Rogado, K. A. Regan, M. A. Hayward, P. Khalifah, T. He, K. Inumaru, S. M. Loureiro, M. K. Haas, H. W. Zandbergen, and R. J. Cava, Nature (London) **410**, 343 (2001).

[8] N. I. Medvedeva, A. L. Ivanovskii, J. E. Medvedeva, and A. J. Freeman, Phys. Rev. B **64**, 020502(R) (2001).

[9] N. Barbero, T. Shiroka, B. Delley, T. Grant, A. J. S. Machado, Z. Fisk, H.-R. Ott, and J. Mesot, Phys. Rev. B **95**, 094505 (2017).

[10] C. Pei, J. Zhang, Q. Wang, Y. Zhao, L. Gao, C. Gong, S. Tian, R. Luo, M. Li, W. Yang *et al.*, Natl. Sci. Rev. **10**, nwad034 (2023).

[11] X. Liu, X. Huang, P. Song, C. Wang, L. Zhang, P. Lv, L. Liu, W. Zhang, J.-H. Cho, and Y. Jia, Phys. Rev. B **106**, 064507 (2022).

[12] Y. Quan, K.-W. Lee, and W. E. Pickett, Phys. Rev. B **104**, 224504 (2021).

[13] E. F. Talantsev, Symmetry **15**, 812 (2023).

[14] J. Lim, A. C. Hire, Y. Quan, J. S. Kim, S. R. Xie, S. Sinha, R. S. Kumar, D. Popov, C. Park, R. J. Hemley *et al.*, Nat. Commun. **13**, 7901 (2022).

[15] P. E. Blöchl, Phys. Rev. B **50**, 17953 (1994).

[16] G. Kresse and J. Furthmüller, Phys. Rev. B **54**, 11169 (1996).

[17] J. P. Perdew, K. Burke, and M. Ernzerhof, Phys. Rev. Lett. **77**, 3865 (1996).

[18] V. L. Deringer, A. L. Tchougréeff, and R. Dronskowski, J. Phys. Chem. A **115**, 5461 (2011).

[19] P. Giannozzi, S. Baroni, N. Bonini, M. Calandra, R. Car, C. Cavazzoni, D. Ceresoli, G. L. Chiarotti, M. Cococcioni, I. Dabo *et al.*, J. Phys.: Condens. Matter **21**, 395502 (2009).

[20] M. Schlipf and F. Gygi, Comput. Phys. Commun. **196**, 36 (2015).

[21] V. Wang, N. Xu, J.-C. Liu, G. Tang, and W.-T. Geng, Comput. Phys. Commun. **267**, 108033 (2021).

[22] L. Xiong, J. Liu, X. Zhang, Q. Tao, and P. Zhu, J. Alloys Compd. **623**, 442 (2015).

[23] H. Klesnar, T. Aselage, B. Morosin, and G. Kwei, J. Alloys Compd. **241**, 180 (1996).

[24] W. Hayami, A. Momozawa, and S. Otani, Inorg. Chem. **52**, 7573 (2013).

[25] See Supplemental Material at http://link.aps.org/supplemental/10.1103/PhysRevB.109.064502 for information on the bonding properties of α-MoB_2 and β-MoB_2, the stability of the phonon spectra under pressure in α-MoB_2, the evolution of electronic loss in Mo under pressure for α-MoB_2 and β-MoB_2, and the electronic structures of the corresponding manipulated phases and AlB_2-type NbB_2 and WB_2.

[26] W. Hanke, J. Hafner, and H. Bilz, Phys. Rev. Lett. **37**, 1560 (1976).

[27] C. M. Varma and W. Weber, Phys. Rev. B **19**, 6142 (1979).

[28] L. Liu, C. Wang, S. Yi, K. W. Kim, J. Kim, and J.-H. Cho, Phys. Rev. B **99**, 140501(R) (2019).

[29] T. A. Manz and N. G. Limas, RSC Adv. **6**, 47771 (2016).

[30] S. Baroni, S. de Gironcoli, A. Dal Corso, and P. Giannozzi, Rev. Mod. Phys. **73**, 515 (2001).

[31] P. B. Allen and R. Dynes, Phys. Rev. B **12**, 905 (1975).

[32] J. P. Carbotte, Rev. Mod. Phys. **62**, 1027 (1990).

[33] F. Abud, L. E. Correa, I. R. Souza Filho, A. J. S. Machado, M. S. Torikachvili, and R. F. Jardim, Phys. Rev. Mater. **1**, 044803 (2017).

[34] C. A. Nunes, D. Kaczorowski, P. Rogl, M. R. Baldissera, P. A. Suzuki, G. C. Coelho, A. Grytsiv, G. André, F. Boureé, and S. Okada, Acta Mater. **53**, 3679 (2005).

[35] L. E. Muzzy, M. Avdeev, G. Lawes, M. K. Haas, H. W. Zandbergen, A. P. Ramirez, J. D. Jorgensen, and R. J. Cava, Physica C (Amsterdam, Neth.) **382**, 153 (2002).

[36] A. Yamamoto, C. Takao, T. Masui, M. Izumi, and S. Tajima, Physica C (Amsterdam, Neth.) **383**, 197 (2002).

[37] R. Escamilla, O. Lovera, T. Akachi, A. Durán, R. Falconi, F. Morales, and R. Escudero, J. Phys.: Condens. Matter **16**, 5979 (2004).

[38] D. P. Young, R. G. Goodrich, P. W. Adams, J. Y. Chan, F. R. Fronczek, F. Drymiotis, and L. L. Henry, Phys. Rev. B **65**, 180518(R) (2002).

[39] M. Mudgel, V. P. S. Awana, G. L. Bhalla, and H. Kishan, Solid State Commun. **147**, 439 (2008).

[40] C. Pei, J. Zhang, C. Gong, Q. Wang, L. Gao, Y. Zhao, S. Tian, W. Cao, C. Li, Z.-Y. Lu *et al.*, Sci. China Phys. Mech. **65**, 287412 (2022).

[41] L. Leyarovska and E. Leyarovski, J. Less Common Met. **67**, 249 (1979).

[42] H. Kotegawa, K. Ishida, Y. Kitaoka, T. Muranaka, N. Nakagawa, H. Takagiwa, and J. Akimitsu, Physica C (Amsterdam, Neth.) **378**, 25 (2002).

[43] H. Takeya, K. Togano, Y. S. Sung, T. Mochiku, and K. Hirata, Physica C (Amsterdam, Neth.) **408**, 144 (2004).

[44] B. Lorenz, R. L. Meng, and C. W. Chu, Phys. Rev. B **64**, 012507 (2001).